THE JOURNAL OF BIOLOGICAL CHEMISTRY
Vol. 277, No. 37, Issue of September 13, pp. 34499–34507, 2002

Printed in U.S.A.

High Resolution Crystal Structures of the Wild Type and Cys-55 → Ser and Cys-59 → Ser Variants of the Thioredoxin-like [2Fe-2S] Ferredoxin from *Aquifex aeolicus**

Received for publication, May 23, 2002, and in revised form, June 25, 2002
Published, JBC Papers in Press, June 27, 2002, DOI 10.1074/jbc.M205096200

Andrew P. Yeh‡, Xavier I. Ambroggio§, Susana L. A. Andrade‡¶, Oliver Einsle‡¶, Claire Chatelet‖, Jacques Meyer‖, and Douglas C. Rees‡¶****

From the ‡Division of Chemistry and Chemical Engineering, the §Division of Biology, and the ¶Howard Hughes Medical Institute, California Institute of Technology, Pasadena, California 91125 and the ‖Département de Biologie Moléculaire et Structurale, Commissariat à l'Energie Atomique, Grenoble F-38054, France

The [2Fe-2S] ferredoxin (Fd4) from *Aquifex aeolicus* adopts a thioredoxin-like polypeptide fold that is distinct from other [2Fe-2S] ferredoxins. Crystal structures of the Cys-55 → Ser (C55S) and Cys-59 → Ser (C59S) variants of this protein have been determined to 1.25 Å and 1.05 Å resolution, respectively, whereas the resolution of the wild type (WT) has been extended to 1.5 Å. The improved WT structure provides a detailed description of the [2Fe-2S] cluster, including two features that have not been noted previously in any [2Fe-2S] cluster-containing protein, namely, pronounced distortions in the cysteine coordination to the cluster and a Cα-H–Sγ hydrogen bond between cluster ligands Cys-55 and Cys-9. These features may contribute to the unusual electronic and magnetic properties of the [2Fe-2S] clusters in WT and variants of this ferredoxin. The structures of the two variants of Fd4, in which single cysteine ligands to the [2Fe-2S] cluster are replaced by serine, establish the metric details of serine-ligated Fe-S active sites with unprecedented accuracy. Both the cluster and its surrounding protein matrix change in subtle ways to accommodate this ligand substitution, particularly in terms of distortions of the Fe_2S_2 inorganic core from planarity and displacements of the polypeptide chain. These high resolution structures illustrate how the interactions between polypeptide chains and Fe-S active sites reflect combinations of flexibility and rigidity on the part of both partners; these themes are also evident in more complex systems, as exemplified by changes associated with serine ligation of the nitrogenase P cluster.

The low potential iron-sulfur (Fe-S) electron carriers known as ferredoxins (Fds)[1] are found in three distinct classes, the [3Fe-4S]/[4Fe-4S] bacterial type Fds, the plant and mammalian type [2Fe-2S] Fds, and the thioredoxin-like [2Fe-2S] Fds (1). The first two classes were discovered nearly 40 years ago (2, 3) and have since been characterized in considerable detail, including by high resolution x-ray crystallography (4, 5). The third class of Fd is more sparsely distributed and, therefore, has not been investigated as thoroughly (1). The best characterized members of that group are [2Fe-2S] Fds from the bacteria *Clostridium pasteurianum* (6), *Azotobacter vinelandii* (7), and *Aquifex aeolicus* (8). The high level of similarity of these proteins allows for easy transfer of structural information among them. For instance, many properties of molecular variants of the *C. pasteurianum* [2Fe-2S] Fd (6, 9, 10) could be rationalized from the crystal structure of *A. aeolicus* Fd4 (11). This structure established the unexpected thioredoxin-like fold of these Fds and confirmed that they are distinct from the other two ferredoxin classes (1). The 2.3 Å resolution of the Fd4 structure, however, was not among the highest currently reported (about 1 Å) for metalloenzymes. Indeed, such high resolution structures are of utmost interest because they bring forth precise geometries of metal sites (4) and may allow description of redox transitions (5). Additional efforts have therefore been made, both on wild type (WT) thioredoxin-like Fds and on several of the molecular variants that were produced over the years (6, 10, 12), with the aim of improving the crystallographic data.

In some modified forms of *C. pasteurianum* Fd, cysteine ligands of the Fe-S cluster were replaced by serine (9, 13). In their reduced $[2Fe\text{-}2S]^{+}$ level, these serine-ligated active sites were found to assume a delocalized mixed valence state having a ground spin state of 9/2 (14, 15). This unprecedented occurrence in binuclear iron-sulfur clusters has stimulated experimental and theoretical work (16, 17). The development of these investigations has been hampered, however, by the absence of structural data on serine-ligated [2Fe-2S] active sites and their environment. Because only the Fd4 from *A. aeolicus* has been crystallized, we have repeated amino acid substitutions in that protein previously performed on *C. pasteurianum* Fd and produced the C55S and C59S variants that contain serine-ligated [2Fe-2S] clusters. We report here the high resolution structures for both of these variants as well as WT protein which provide accurate metric details for serine-ligated Fe-S clusters in proteins.

EXPERIMENTAL PROCEDURES

Protein Samples—Fd4 from *A. aeolicus* was purified as described by Chatelet *et al.* (8). The C55S and C59S variants were prepared by site-directed mutagenesis as described for the C56S and C60S counterparts from *C. pasteurianum* (13). The mutagenic oligonucleotides were

* This work was supported by National Institutes of Health Grant GM45062 (to D. C. R.) and by a predoctoral fellowship from the National Science Foundation (to X. I. A.). The costs of publication of this article were defrayed in part by the payment of page charges. This article must therefore be hereby marked "*advertisement*" in accordance with 18 U.S.C. Section 1734 solely to indicate this fact.

The atomic coordinates and structure factors (code 1M2A, 1M2B and 1M2D) have been deposited in the Protein Data Bank, Research Collaboratory for Structural Bioinformatics, Rutgers University, New Brunswick, NJ (http://www.rcsb.org/).

** To whom correspondence may be addressed: Division of Chemistry and Chemical Engineering, 147-75CH, California Institute of Technology, Pasadena, CA 91125 (for D. C. R.). E-mail: dcrees@caltech.edu or DBMS-BECP, CEA-Grenoble, 38054 Grenoble, France (for J. M.). E-mail: jacques.meyer@cea.fr.

[1] The abbreviations used are: Fd(s), ferredoxin(s); Fd4, [2Fe-2S] ferredoxin 4 from *A. aeolicus*; MES, 4-morpholineethanesulfonic acid; WT, wild type.

TABLE I
Summary of data collection and refinement statistics

	WT	C55S	C59S
Data collection statistics			
Maximum resolution (Å)	1.50	1.25	1.05
Wavelength (Å)	0.9918	0.8860	0.9580
Total reflections	98,554	183,676	358,550
Unique reflections	27,758	48,256	77,950
Completeness (%)[a]	98.9 (97.1)	99.7 (99.5)	95.6 (92.0)
$I/\sigma(I)$	7.8 (1.5)	28.5 (3.8)	38.2 (6.4)
R_{sym} (%)[b]	5.1 (40.4)	4.7 (26.1)	3.5 (21.6)
Refinement statistics			
Resolution limits (Å)	31.5–1.50	44.3–1.25	31.2–1.05
R-factor[c]	0.184	0.144	0.138
R-free	0.216	0.196	0.162
Estimated coordinate error (Å)[d]	0.09	0.05	0.03
RMS deviations from ideal values			
Bond lengths (Å)	0.024	0.015	0.017
Bond angles (°)	2.192	3.056	2.666
Dihedral angles (°)	25.11	26.48	26.38
Improper torsion angles (°)	1.60	1.64	1.83
Average temperature factor (Å^2)			
Protein	22.1, 20.6	21.0, 19.9	18.1, 16.1
Iron-sulfur	13.0, 12.8	12.9, 12.2	9.5, 9.7
Water	36.8	39.3	31.9
Zinc	37.1		
Sulfate	44.3		
Ramachandran plot,[e] residues in			
Most favored regions (%)	90.2	93.2	93.2
Additional allowed regions (%)	9.1	6.8	6.8
Generously allowed regions (%)	0.6	0.0	0.0
Disallowed regions (%)	0.0	0.0	0.0

[a] Numbers in parentheses correspond to values in the highest resolution shell.
[b] $R_{sym} = (\Sigma_{hkl}\Sigma_i|I_i(hkl) - < I(hkl) > |)/(\Sigma_{hkl}\Sigma_i\ I(hkl))$.
[c] R-factor = $\Sigma(|F_{obs}| - |F_{calc}|)/\Sigma|F_{obs}|$, R-free is the R-factor calculated for a 3% test set of reflections excluded from the refinement calculation.
[d] Coordinate errors were obtained from the diffraction component precision index, calculated from the values of R-free by the method of Cruickshank (42).
[e] As determined by PROCHECK (43).

5′-cacgcgttcatgGaaccggtgggag-3′ (hybridizing to the coding strand, mutated base in underlined uppercase) and 5′-ggttgcatgaacgcgtCtatgatgggaccg-3′ (hybridizing to the noncoding strand), for C55S and C59S, respectively. The mutated genes were overexpressed in *Escherichia coli*, and the C55S and C59S proteins were purified as described for the WT (8).

Crystallization—Crystals of oxidized WT, C55S, and C59S Fd4 were prepared by the sitting drop vapor diffusion method. Although anaerobic conditions were employed to minimize degradation of the cluster by exposure to atmospheric oxygen, no reductants were present during the crystallizations, so that the proteins should remain in the oxidized state. In the case of C55S, crystals were obtained by equilibrating 2 μl of reservoir solution and 2 μl of ~83 mg/ml Fd4 C55S (in 20 mM Tris-HCl buffer at pH 8.0 and 0.2 M NaCl) against a reservoir solution containing 30% (w/v) polyethylene glycol 4000, 0.2 M ammonium acetate, and 0.1 M sodium acetate at pH 4.6. Crystals of Fd4 C59S were obtained by equilibrating 2 μl of reservoir solution and 2 μl of ~67 mg/ml Fd4 C59S (in 20 mM Tris-HCl buffer at pH 8.0 and 0.2 M NaCl) against a reservoir solution containing 1.0 M 1,6-hexanediol, 0.01 M cobalt chloride and 0.1 M sodium acetate at pH 4.6. WT Fd4 was crystallized by equilibrating 2 μl of ~10 mg/ml Fd4 (in 10 mM Tris-HCl buffer at pH 8.0 and 0.2 M NaCl) and 2 μl of reservoir solution against a reservoir solution containing 0.01 M zinc sulfate heptahydrate, 0.1 M MES buffer at pH 6.5, and 25% polyethylene glycol monomethyl ether 550. Despite the different crystallization conditions, in all three cases nearly isomorphous crystals were obtained in space group *C2* (C55S: a = 67.3 Å, b = 59.8 Å, c = 46.9 Å, β = 109.8°; C59S: a = 67.3 Å, b = 59.8 Å, c = 46.8 Å, β = 109.3°; WT: a = 67.2 Å, b = 59.8 Å, c = 47.2 Å, β = 110.3°), with one dimeric Fd4 molecule/asymmetric unit.

Data Collection, Structure Determination, and Refinement—Diffraction data to 1.25 Å resolution for C55S and 1.05 Å resolution for C59S were collected under cryogenic conditions on beamline 9-2 at the Stanford Synchrotron Radiation Laboratory on an Area Detector Systems Corp. Quantum-4 CCD detector controlled by the distributed control system software BLU-ICE. C55S and C59S data sets were processed and scaled using DENZO and SCALEPACK (18). Diffraction data to 1.5 Å resolution for WT Fd4 were collected under cryogenic conditions at the Stanford Synchrotron Radiation Laboratory beamline 9-2 on an Area Detector Systems Corp. Quantum-315 CCD detector and were processed and scaled using MOSFLM and SCALA (19). A summary of the data collection statistics is listed in Table I.

The Fd4 C55S structure was solved by molecular replacement using EPMR (20) with the original WT Fd4 structure determined at 2.3 Å resolution (11) as the search model. Multiple rounds of positional refinement and individual isotropic B-factor refinement with crystallography NMR software (21) were alternated with model rebuilding in the molecular graphics program O (22) against 2 $F_o - F_c$ σ_a-weighted and $F_o - F_c$ σ_a-weighted maps (23). The [2Fe-2S] cluster geometry was not restrained during refinement. Upon solvent addition and completion of refinement with CNS, positional and anisotropic B-factor refinements of the model were performed using the programs SHELX97 (24) and REFMAC5 (25), which resulted in a final R-factor and R-free of 14.4 and 19.6%, respectively. A final round of refinement in SHELX97 yielded the standard uncertainties in atomic coordinates, bond lengths, and angles. The final Fd4 C55S model comprises two subunits (2 × 101 residues, 1,575 atoms), two [2Fe-2S] clusters (8 atoms), and 215 water molecules. Because of the absence of electron density for the first 2 residues at the N terminus and the last 7 residues at the C terminus, these residues were not modeled.

The Fd4 C55S model without water molecules was used as the starting model for the Fd4 C59S model. The Fd4 C59S model was refined using a protocol similar to that outlined above for Fd4 C55S to an R-factor and R-free of 13.8 and 16.2%, respectively. As with Fd4 C55S, no electron density was present for the first 2 residues at the N terminus, and the last 7 residues at the C terminus were absent. The final Fd4 C59S model consists of two subunits (2 × 101 residues, 1,576 atoms), two [2Fe-2S] clusters (8 atoms), and 198 water molecules.

The Fd4 C55S model without water molecules was also used as the starting model for the high resolution WT structure. The model was refined using CNS (21) with a protocol similar to that described above to an R-factor and R-free of 18.4 and 21.6%, respectively. The cluster geometry was not restrained during refinement. During the solvent addition process, 4 zinc ions and 1 sulfate anion were modeled into difference electron density peaks that were significantly higher than those corresponding to the water molecules. In contrast to the variant structures, the WT temperature factors were not refined anisotropically because of the lower resolution of the data. The final model comprises two subunits (103 residues in subunit A, 101 residues in subunit B,

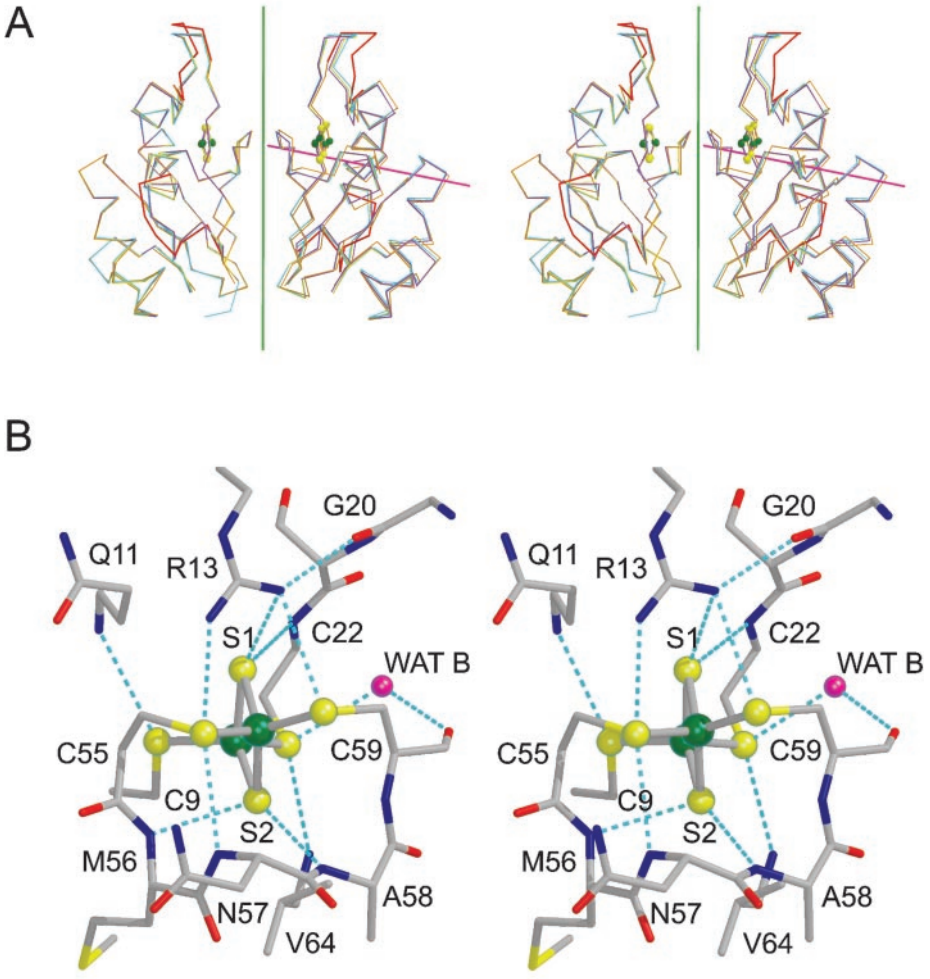

FIG. 1. *A*, stereoview of superimposed Fd4 dimers from the original WT (*orange*), current WT (*cyan*), C55S (*yellow*), and C59S (*purple*) structures. The A subunits of these molecules were used in the superposition. The *green line* denotes the 2-fold rotation axis relating subunits A (*left*) and B (*right*) in a dimer; the *magenta line* corresponds to the axis about which the B subunit of the previous WT structure (11) is rotationally shifted relative to the B subunit of the current WT form. This rigid body rotational shift as well as regions of the old form which differ significantly from the new form (residues 13–20 and 39–46, *highlighted* in *red*) are likely the results of the different crystal packing between the two WT forms. *B*, stereoview of the [2Fe-2S] cluster and its immediate environment in WT Fd4, illustrating the hydrogen bonding network involving the cluster, ligands, and surrounding residues, with the exception of the Cys-55 CαH-Cys-9 Sγ hydrogen bond detailed in Fig. 2*A*. Iron and sulfur atoms are colored *green* and *yellow*, respectively. Fe1 is coordinated by Cys-9 and Cys-22, whereas Fe2 is ligated by Cys-55 and Cys-59.

1,590 atoms), two [2Fe-2S] clusters (8 atoms), 187 water molecules, 4 zinc ions, and 1 sulfate anion. Final refinement statistics for all three structures are listed in Table I.

RESULTS AND DISCUSSION

Wild Type Fd4

Overall Structure—The WT and serine-substituted forms of Fd4 analyzed in this study were crystallized in a monoclinic space group, *C2*, which is distinct from the original tetragonal form solved at 2.3 Å resolution (11). As observed originally, the current structure of WT Fd4 determined at 1.5 Å resolution exists as a homodimer, with each monomer adopting a thioredoxin-like fold (Fig. 1*A*). The two noncrystallographic symmetry-related subunits are nearly identical, with a root mean square deviation of 0.27 Å between 101 Cα atoms. As a consequence of the differences in crystal packing between the original and present WT structures, the two monomers in the Fd4 dimer undergo a slight rigid body shift relative to each other (Fig. 1*A*). With the A subunits of both WT forms superimposed, the shift in the B subunit of the new WT form relative to that of the old form can be characterized quantitatively as a 3.8° rotation about an axis oriented ~74° from the 2-fold rotation axis relating subunits in the dimer. The axis about which this 3.8° rotation occurs passes near residue Thr-B53, which along with Pro-B52, Gly-B54, and the corresponding residues in subunit A, form a short stretch of antiparallel β-sheet which stabilizes the dimer interface. As a result of this change in dimer packing, the hydrogen bonding geometries of residues in this antiparallel arrangement of β-strands are slightly modified. Because cluster ligand Cys-55 is adjacent to this region, it is possible that these alterations in subunit-subunit packing could be coupled to changes in cluster environment. The differences in crystal interactions are also reflected in changes in conformations in two flexible loop regions spanning residues 13–20 and residues 39–46 (Fig. 1*A*), the former of which is near the cluster ligands Cys-9 and Cys-22.

Iron-Sulfur Cluster—The [2Fe-2S] cluster, located near the surface of each monomer, is coordinated by 4 cysteines, with Cys-9 and Cys-22 ligating Fe1 and Cys-55 and Cys-59 ligating Fe2 (Fig. 1*B*). At the resolution of the current study, it was possible to conduct the refinement without restraining the cluster geometry, resulting in stereochemical parameters that are both more accurate and also less biased than in the previous WT model.

A [2Fe-2S] cluster coordinated by four sulfhydryl groups may be idealized as a framework consisting of two edge-sharing tetrahedral iron sites with a planar Fe_2S_2 inorganic core. The geometries of real [2Fe-2S] clusters, as observed in both model compounds and in proteins, generally reflect this expectation, although deviations from this idealization are evident (26). Table II summarizes the average stereochemical parameters for [2Fe-2S] clusters in the Fd4 structures described here as well as in proteins refined at high resolution and in model compounds. In general, the bond distances and angles observed in protein-bound [2Fe-2S] clusters agree well with each other and with model compounds. A notable deviation from the idealized symmetry in the protein-bound clusters, however, is the nonplanarity of the Fe_2S_2 core, which can be characterized by the average absolute value of ~175° for the Fe-S-S-Fe torsion

TABLE II

Average stereochemical parameters for Fd4 structures (from Table I)

Protein standards are the average values for four independent [2Fe-2S] clusters coordinated by four cysteine ligands in protein structures refined at resolutions ≤1.4 Å. These structures include PDB entries 1QT9, 1AWD, and the two distinct clusters in 1HLR (5, 33, 38). The model compound parameters are derived from the structure of $(Fe_2S_2(SC_6H_4CH_3)_4)^{2-}$ (44).

Parameter	WT	C55S	C59S	Protein standards	Model compound
Bonds (Å)					
Fe-S	2.23	2.24	2.23	2.23 ± 0.03	2.201
Fe-Fe	2.73	2.69	2.69	2.73 ± 0.02	2.691
S-S	3.52	3.59	3.55	3.51 ± 0.04	3.483
Angles (°)					
S-Fe-S	104.5	106.2	105.6	104.3 ± 1.8	104.6
Fe-S-Fe	75.4	73.5	74.4	75.5 ± 1.0	75.4
9Sγ-Fe-22Sγ	104.6	105.1	106.1	105.1 ± 1.7	111.2
55S/Oγ-Fe-59S/Oγ	90.5	96.4	99.1		
|Fe-S-S-Fe| torsion angle	173	171	177	175	180

TABLE III

Cluster geometry in molecules A and B for WT, C55S, and C59S Fd4

Numbers in parentheses correspond to standard uncertainties in the last digit. Because of the lower resolution of the WT structure, coordinate uncertainties of the individual atoms were not calculated.

Parameter	Residue	WT		C55S		C59S	
		A	B	A	B	A	B
Bonds (Å)							
Fe1-Fe2		2.74	2.72	2.692	2.681	2.697	2.690
S1-S2		3.52	3.52	3.590	3.592	3.548	3.546
Fe1-S1		2.24	2.22	2.262(7)	2.244(7)	2.216(4)	2.214(3)
Fe1-S2		2.21	2.19	2.215(9)	2.222(8)	2.215(4)	2.217(4)
Fe2-S1		2.23	2.24	2.20(1)	2.200(9)	2.232(4)	2.220(4)
Fe2-S2		2.25	2.25	2.305(8)	2.308(8)	2.217(4)	2.253(4)
Sγ-Fe1	C9	2.27	2.26	2.330(7)	2.328(6)	2.303(4)	2.302(4)
Sγ-Fe1	C22	2.31	2.28	2.302(8)	2.306(8)	2.302(4)	2.304(4)
Sγ-Fe2	C55	2.34	2.37	1.97(1)	2.01(2)	2.318(4)	2.315(5)
Sγ-Fe2	C59	2.29	2.33	2.300(9)	2.296(9)	1.940(9)	1.942(8)
Angles (°)							
S1-Fe1-S2		104.8	106.0	106.7(3)	107.1(3)	106.4(2)	106.3(2)
S1-Fe2-S2		103.7	103.3	105.6(3)	105.6(3)	104.6(2)	104.9(2)
Fe1-S1-Fe2		75.6	75.1	74.2	74.2	74.7	74.7
Fe1-S2-Fe2		75.7	75.3	73.1	72.5	74.3	74.0
Sγ-Fe1-Sγ	C9/C22	105.0	104.3	105.7(3)	104.6(2)	106.1(1)	106.1(1)
O/Sγ-Fe2-O/Sγ	C/S55-C/S59	90.5	90.4	96.6(5)	96.3(5)	100.0(3)	98.2(3)
Sγ-Fe1-S1	C9	105.4	106.4	103.9(3)	104.6(3)	104.2(1)	104.4(1)
Sγ-Fe1-S2	C9	116.7	116.2	115.7(3)	115.2(2)	116.5(1)	116.1(1)
Sγ-Fe1-S1	C22	115.5	113.7	115.7(3)	114.5(3)	115.4(1)	115.4(1)
Sγ-Fe1-S2	C22	109.9	110.6	109.5(3)	110.9(3)	108.5(1)	108.9(1)
O/Sγ-Fe2-S1	C/S55	115.4	115.7	109.2(6)	109.6(6)	114.7(2)	114.9(2)
O/Sγ-Fe2-S2	C/S55	112.7	113.5	112.7(5)	112.0(5)	112.8(1)	112.7(2)
O/Sγ-Fe2-S1	C/S59	113.2	112.2	110.8(4)	111.8(4)	107.6(3)	107.9(3)
O/Sγ-Fe2-S2	C/S59	121.8	122.3	121.6(3)	121.2(3)	117.5(3)	118.6(3)
Torsion Angle (°)							
Fe1-S1-S2-Fe2		−174.4	−172.0	−170.8	−170.6	−176.7	−176.7

angle, where 180° would correspond to exact planarity. For further comparison, the Fe_2S_2 unit present in [4Fe-4S] clusters is significantly more nonplanar than in [2Fe-2S] clusters, with an average value for this torsion angle of only 162.0° (27). The pronounced puckering of this unit in [4Fe-4S] clusters reflects primarily a more compressed Fe-S-Fe angle (71.7°) relative to [2Fe-2S] clusters (75.5°).

A detailed examination of the geometrical parameters of the [2Fe-2S] cluster in WT Fd4 (Table III) reveals two pronounced outliers: (i) the relatively small Cys-55 Sγ-Fe2 Cys-59 Sγ bond angle and (ii) a relatively long Cys-55 Sγ-Fe2 bond. The Cys-55 Sγ-Fe2 Cys-59 Sγ angle averages 90.5° in the two crystallographically independent subunits of WT Fd4, a value that is significantly smaller than the average Cys-9 Sγ-Fe2-Cys-22 Sγ angle of 104.6° observed in the same structure and the consensus value of 105.1° observed in other well refined [2Fe-2S] protein structures (Table II). The more compressed Cys-55 Sγ-Fe2-Cys-59 Sγ angle has not been observed previously in other well refined ferredoxins with Cys ligands but is similar to the His Nδ-Fe-His Nδ bond angles of ~94° observed in Rieske type [2Fe-2S] clusters (28, 29). The other unusual feature of the Fd4 cluster geometry involves the Cys-55 Sγ-Fe2 bond, which is longer on average by ~0.06 Å than the other three Fe-Sγ bonds (Table III). Constraints on the position of Cys-55 may contribute to this elongated bond because the residues around Cys-55 are well defined and appear to be relatively rigid, as reflected by the lower average temperature factors in this region (14.9 $Å^2$ for residues 53–57 *versus* 21.4 $Å^2$ for all protein atoms). An associated phenomenon may be the increased distortion of the peptide bond torsion angles (ω) of the residues surrounding Cys-55, particularly Thr-53, Met-56, and Ala-58, whose ω torsion angles are on average 166.0°, 171.8°, and 189.1°, respectively (2.4, 1.4, and 1.6 standard deviations from the ideal value of 180°). With an average Fe1-S1-S2-Fe2 torsion angle of –173°, the extent of nonplanarity of the [2Fe-2S] cluster in WT Fd4 is comparable with those observed in other well refined [2Fe-2S] protein structures.

Cys-55 also participates in an unusual interaction involving the probable formation of a Cα-H-Sγ hydrogen bond between the Cys-55 Cα-H and Cys-9 Sγ (Fig. 2*A*). This interaction is

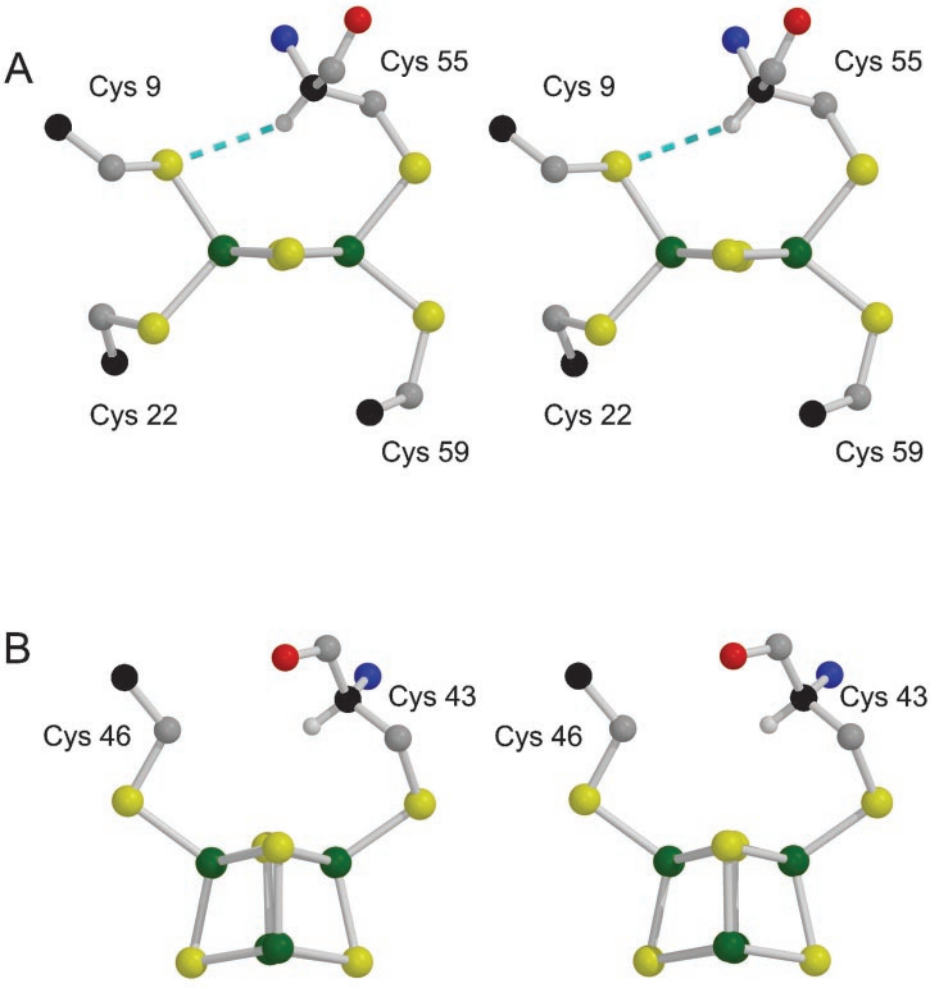

FIG. 2. **Stereoviews of the potential interactions between Cys ligands across the Fe_2S_2 face of iron-sulfur clusters.** *A*, the [2Fe-2S] cluster of Fd4, illustrating the conformation of Cys-55 in which the Cα-H group is positioned over the cluster to hydrogen bond (*dashed line*) with the Cys-9 Sγ. *B*, a similar configuration is observed in the high potential iron protein from *C. vinosum* ((45) PDB 1CKU). Whereas Cys-43 and Cys-46 have the same general relationship to the common face of the [4Fe-4S] cluster in this protein, the increased pucker of the Fe_2S_2 core precludes the formation of a Cα-H-Sγ hydrogen bond. For clarity, two of the cysteine ligands in high potential iron protein have been omitted from the figure. Iron, sulfur, nitrogen, oxygen, and Cα atoms are colored *green*, *yellow*, *blue*, *red*, and *black*, respectively.

identified on the basis of the Cys-55 Cα- Cys-9 Sγ and the Cys-55 Cα-H-Cys-9 Sγ distances of 3.6 and 2.7 Å, respectively, with a Cα-H-Sγ angle of 149°. For the purposes of this calculation, hydrogen positions were generated with the CCP4 program HGEN (19). Identification of this interaction as a hydrogen bond is consistent with the criteria used to identify potential Cα-H-O hydrogen bonds (a Cα-H-O distance of 2.7 Å (30), which does not take into account the increased van der Waals radius of S relative to O). To our knowledge, this type of hydrogen bond has not been described previously in [2Fe-2S] cluster-containing proteins, although they have been described elsewhere (31, 32). For this interaction to occur, the Cys-55 Cα must be positioned over the [2Fe-2S] cluster, with the hydrogen directed toward the Sγ ligand (Cys-9) of the adjacent iron. Examination of the [2Fe-2S] cluster-containing proteins used in the analysis for Table II, as well as of [4Fe-4S] cluster-containing proteins described in Ref. 27, suggests that there are two related side chain conformations that can potentially achieve this interaction. These conformations may be defined in terms of three torsion angles: χ_1, the N-Cα-Cβ-Sγ angle; χ_2, which describes the Cα-Cβ-Sγ-Fe angle; and χ_3, which describes the Cβ-Sγ-Fe-S angle. Because there are either two or three cluster sulfides that can be used to define this latter angle, for [2Fe-2S] and [4Fe-4S] clusters, respectively, the convention that will be used is to adopt the angle whose absolute value is closest to 0°. With these definitions, the side chain conformations that place the ligand Cα over the ring are (χ_1, χ_2, χ_3) ~(180°, 60°, 30°) and (−60°, −60°, −30°); the positions of the Cα, Cβ, and Sγ atoms for these two conformations are related by a mirror plane that passes through the two iron sites, perpendicular to the Fe_2S_2 plane (Fig. 2). The first solution corresponds to that observed for Cys-55 of Fd4, whereas the latter is observed in [4Fe-4S] cluster-containing proteins such as high potential iron proteins. In the latter case, however, the Cα-H-Sγ bond cannot be formed because the significant pucker in the Fe_2S_2 moiety of [4Fe-4S] clusters leads to an increase of the Cα-Sγ distance to ~5.3 Å, a separation which is too great for this interaction to occur (Fig. 2*B*).

With the exception of the Cα-H-Sγ interaction just described, the hydrogen bonding network in the [2Fe-2S] cluster environment of Fd4 (Table IV) is altogether not unlike that occurring in plant type Fds (5, 33), which assume distinct protein folds. It is interesting to note that in both cases, the Sγ atoms of the cysteine ligands to the more reducible iron are more solvent exposed and are collectively involved in a larger number of hydrogen bonds than the cysteine ligands of the nonreducible iron (9, 14, 34). The hydrogen bonding network around the cluster in Fd4 does appear to exhibit some variability, as evidenced by the ability of Arg-13 in subunit B to adopt two different conformations: one in which the guanidino moiety can donate a hydrogen bond to Cys-59 Sγ and another in which this group is far enough away such that no such interaction can occur. In the former conformation, Arg-13 is in a position that could shield the [2Fe-2S] cluster from the solvent.

Structural Effects of the Cysteine to Serine Substitutions

Previous spectroscopic characterizations of the C56S and C60S variants of the homologous [2Fe-2S] ferredoxin from *C. pasteurianum* revealed that substitution of the cysteine with a serine at either of these positions resulted in stable protein

TABLE IV
Hydrogen bonding geometry in the [2Fe-2S] cluster environment

D (donor), A (acceptor); separation distance is measured in Å. Although not specifically indicated, the D-H-A angles for these interactions are all >125 °.

D	A	WT		C55S		C59S	
		A	B	A	B	A	B
		D-A	D-A	D-A	D-A	D-A	D-A
C22N	S1	3.39	3.44	3.43	3.43	3.40	3.40
M56N	S2	3.26	3.29	3.35	3.34	3.34	3.35
A58N	S2	3.55	3.55	3.57	3.45	3.63	3.58
R13NH1	S1	3.54	3.42				
Wat A	S1			3.56	3.62	3.76	3.73
Q11N	Cys9Sγ	3.58	3.52	3.57	3.48	3.55	3.54
V64N	Cys22Sγ	3.51	3.6	3.48	3.53	3.54	3.57
Wat B	Cys22Sγ	3.11	3.19	3.19	3.25	3.30	3.28
R13NH2	55S/Oγ	3.17	3.06	3.68	3.74	3.42	3.48
N57N	55S/Oγ	3.25	3.29	3.51	3.54	3.30	3.35
Wat C	55S/Oγ					3.84	3.73
Wat D	55S/Oγ			2.76			
Wat E	55S/Oγ					3.63	4.15
R13NH1	59S/Oγ	3.46	3.39				
Wat A	59S/Oγ			3.36	3.35	2.93	2.95
Wat C	59S/Oγ					2.63	2.58
Wat D	59S/Oγ			3.77			
Wat F	59S/Oγ	3.45	3.42				
Wat G	59S/Oγ		3.67		3.79		

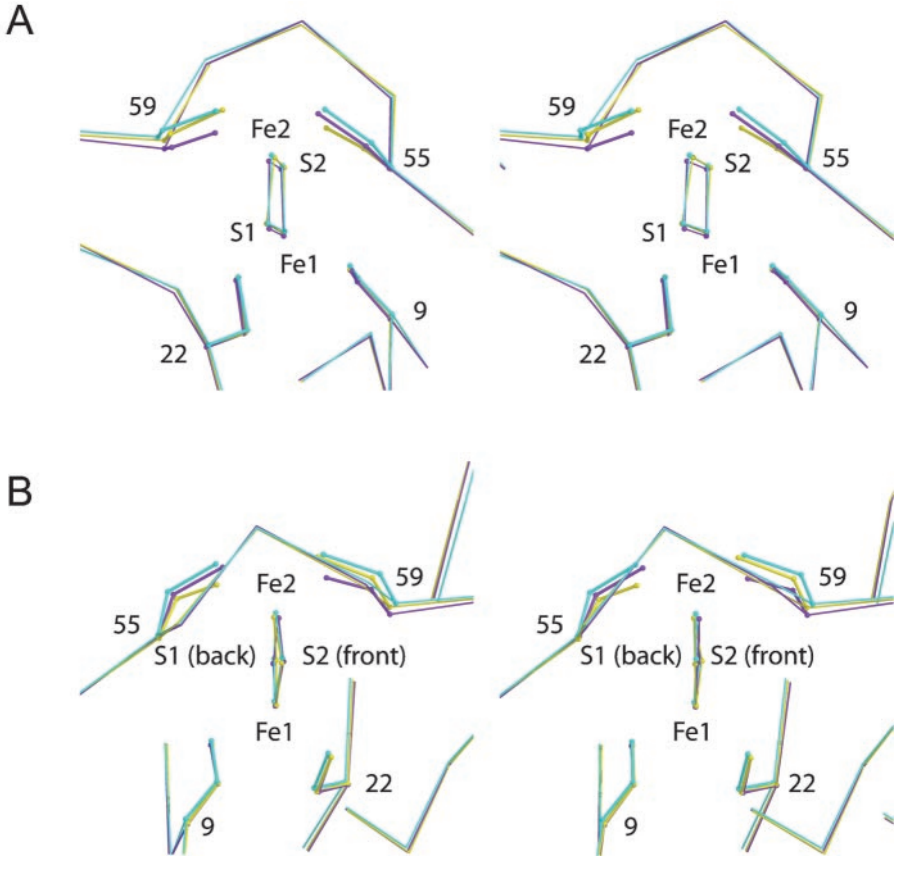

FIG. 3. *A*, stereoview of the [2Fe-2S] cluster and its ligands from the WT (*cyan*), C55S (*yellow*), and C59S (*purple*) structures upon superposition of the corresponding 101 Cα atoms of the three structures, showing the varying degree of positional shifts that occur in the inorganic core as well as residues 55 and 59 caused by the cysteine to serine substitutions. *B*, stereoview of the same region, viewed from a direction perpendicular to that in *A*, illustrates the varying degrees to which the inorganic core is distorted in each structure. The color scheme is the same as in *A*.

with serine-coordinated [2Fe-2S] clusters (9, 13). The high resolution crystal structures of the corresponding C55S (1.25 Å) and C59S (1.05 Å) mutated forms of the *A. aeolicus* Fd4 confirm this serine coordination and furthermore allow the consequences of this serine substitution on the [2Fe-2S] cluster geometry to be accurately assessed.

The overall structures of both C55S and C59S Fd4 are nearly identical to that of the WT structure of Fd4 at 1.5 Å resolution (Fig. 1*A*). The root mean square deviations between the corresponding subunits A and B of WT and C55S are 0.17 and 0.16 Å and of WT and C59S are 0.18 and 0.23 Å. Although there are no gross perturbations between the mutant and WT structures, there are subtle differences in the cluster geometry and its local environment resulting from the cysteine to serine substitutions. For all three structures, the distances and angles pertaining to the [2Fe-2S] cluster and hydrogen bonds involving the cluster are provided in Tables II and III.

As expected, the overall geometry of the cluster in both mutated forms is very similar to that of WT Fd4, with the most pronounced differences being the shorter length of the Fe2-Oγ bond in both variants compared with that of the Fe-Sγ bond in WT (Table III and Fig. 3). The average Fe2-Oγ distance is 1.99 Å

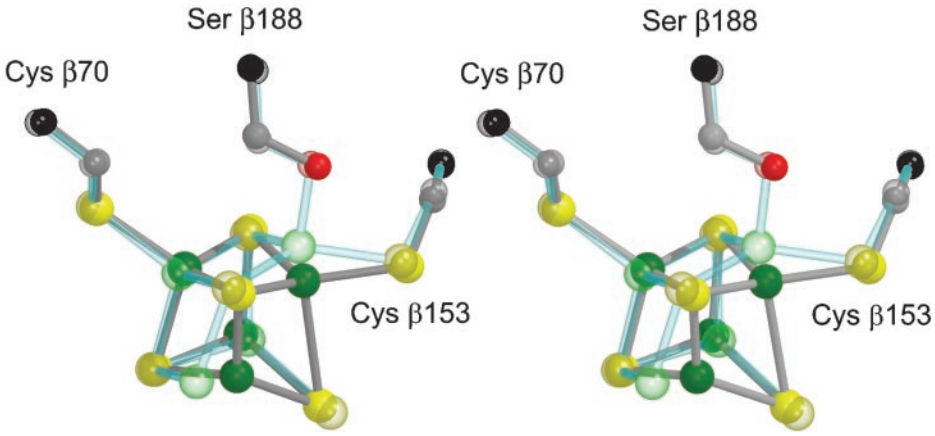

FIG. 4. **Stereoview comparing the P cluster of nitrogenase in the oxidized (*transparent ball-and-stick* model in *cyan*) and reduced (*solid ball-and-stick* model in *gray*) states (39, 40).** In the oxidized state, one of the irons is coordinated by the side chain of Ser-β188, whereas in the reduced state this iron is shifted and coordinates an inorganic sulfur in the cluster instead. The coloring scheme is as in Fig. 3. PDB entries 2MIN (oxidized) and 3MIN (reduced) were used for this figure.

in C55S and 1.94 Å in C59S, whereas the average length of the Fe-Sγ bonds in WT Fd4 is 2.31 Å. The Fe-O bond lengths in these structures are comparable with those seen in the structures of an *Anabaena* [2Fe-2S] ferredoxin in which one of the cysteine ligands, Cys-49, was replaced by a serine (34) (PDB 1QOA; average Fe-O bond length of 1.91 Å) as well as of *C. pasteurianum* rubredoxin in which one of the iron ligands, Cys-42, was replaced by a serine (35) (PDB 1BE7; Fe-O bond length of 1.94 Å (36)). These bonds, however, are shorter than the value of 2.16 Å reported for the Fe-O bond observed in the structure of a C77S ligand-exchanged form of the *Chromatium vinosum* [4Fe-4S] high potential iron protein (37). The relatively longer Fe-O bond length observed in that structure was speculated to result from the structural rigidity of the polypeptide backbone. Aside from the shorter Fe-O bond length, also associated with the substitution of the Ser Oγ for Cys Sγ is an increase of ~6–9° in the Oγ-Fe-Sγ angle relative to the compressed values observed for the corresponding Cys-55 Sγ-Fe-Cys-59 Sγ angle in WT (Table II). In the C49S variant of the *Anabaena* ferredoxin (34), an increase in the Oγ-Fe-Sγ angle of ~7° on average was observed relative to the native Sγ-Fe-Sγ value (5), whereas changes from approximately −4° to +5° in the three Oγ-Fe-Sγ angles relative to the corresponding Sγ-Fe-Sγ angles were observed (36) in the C42S variant of *C. pasteurianum* rubredoxin (35).

Accommodation of the cysteine to serine substitution in both C55S and C59S is facilitated by structural changes in the protein backbone/side chain as well as the inorganic iron-sulfur core itself. The main displacements are those of the Oγ and Fe2 atoms toward each other as well as a somewhat lesser movement of the Sγ atom of the other Fe2 ligand, which follows the movement of the iron. The details of these structural changes in each case (C55S and C59S) differ, however, most likely as a result of the different flexibility of the polypeptide chain near each of these cysteine residues. In the case of C55S, adaptation to the substitution occurs primarily through movement of the Ser-55 Oγ atom toward the iron-sulfur core (Fig. 3). Relative to the position of the corresponding Cys-55 Sγ atom in the WT structure, the Ser-55 Oγ atom shifts by ~0.64 Å in the C55S structure, with little accompanying movement in the backbone atoms of this residue. There is also a ~0.2 Å shift of Fe2 toward the Ser-55 Oγ atom to which it is coordinated, which results in an even more pronounced distortion from planarity of the [2Fe-2S] core than in the WT structure, as reflected by the average Fe1-S1-S2-Fe2 torsion angle of −171° compared with the WT value of −173°. Other changes in the cluster geometry include a decrease of ~0.04 Å in the Fe1-Fe2 distance which is associated with changes of approximately +1° and –2° in the average S-Fe-S and Fe-S-Fe angles, respectively (Table II). The third structural change that arises from the C55S mutation involves Cys-59, the other Fe2 ligand. As a result of the slight movement of Fe2 toward Ser-55, both the side chain and main chain atoms of Cys-59 are pulled toward Fe2 to maintain an Fe2-Sγ bond length of ~2.3 Å. The greater degree to which Cys-59 is structurally perturbed compared with Ser-55, particularly in terms of movement of the backbone atoms, highlights the apparently greater structural rigidity in the region surrounding residue 55.

The main structural perturbations resulting from the C59S mutation, as with C55S, also involve residues 55, 59, and Fe2 of the inorganic core. The shorter Fe-O bond in the C59S structure is accommodated by the movement of Ser-59 and Fe2 toward each other (Fig. 3). Relative to the corresponding atoms in the WT structure (*i.e.* Cys-59 Cα and Sγ), the Cα and Oγ atoms of Ser-59 have shifted 0.42 and 0.70 Å toward Fe2, whereas Fe2 has shifted by ~0.17 Å toward Ser-59. As a result, the Fe-S core becomes more planar (torsion angle of −177°), as opposed to the increase in distortion observed in C55S (Table II). Aside from a shift in the Fe2 position, the only other discernible difference in the inorganic core is a decrease in the Fe1-Fe2 distance by ~0.04 Å, similar to what was observed in the C55S structure. And as in C55S, this compression is associated with changes of approximately +1° and –1° in the values of the S-Fe-S and Fe-S-Fe angles, respectively. Reflecting the same trends as seen for the Cys-55 Sγ-Fe and Cys-59 Sγ-Fe bonds in the WT protein, the Fe-O bonds in C59S are shorter than those in C55S by an average of ~0.05 Å (Table III). Again, a likely explanation for this observation is the greater flexibility in the region surrounding position 59 compared with that surrounding position 55, as discussed previously.

Hydrogen bonding interactions between the protein and the [2Fe-2S] cluster in the serine variants are generally similar to those observed in the WT structure (Table IV). One distinction, however, is that in both the C55S and C59S structures, the side chain of Arg-13 adopts the minor conformation of the WT structure, with a water molecule forming a hydrogen bond to the Cys-59 Sγ/Oγ atom in place of the Arg-13 guanidino group.

CONCLUSIONS

The crystal structure of the WT form of Fd4 at the higher resolution of 1.5 Å reveals metric details of the [2Fe-2S] cluster which could not be assigned confidently in the initial study at 2.3 Å resolution. Some of these features are shared with other

structurally characterized [2Fe-2S] proteins (5, 33, 38), even though the polypeptide folds are distinct. For instance, in the available high resolution structures, the Fe_2S_2 inorganic cores of most protein-bound clusters are distorted from planarity by ~5–10°. The active site moiety containing the reducible iron (55Sγ-Fe2–59Sγ in the case of *A. aeolicus* Fd4) is more solvent exposed and is involved in a larger number of hydrogen bonds than the other moiety (9, 14, 34). Furthermore, as noted in the *Anabaena* [2Fe-2S] ferredoxin (5), the Fe-S bond lengths involving the more solvent-exposed Fe tend to be slightly longer than those to the buried site (Table III). The [2Fe-2S] active site of *A. aeolicus* Fd4 is also notable for features that have not been observed previously in any [2Fe-2S] protein: the long Cys-55 Sγ-Fe2 bond, the compressed Cys-55 Sγ-Fe2-Sγ-Cys-59 angle, and the Cys-55 Cα-H-Cys-9 Sγ hydrogen bond. These unique features are at least in part consequences of the rigid protein environment around residue 55 and are most probably relevant to the spectroscopic idiosyncrasies of thioredoxin-like [2Fe-2S] Fds, particularly in the ways in which they differ from the plant type [2Fe-2S] Fds (1, 9).

The structures of the C55S and C59S variants have been obtained at even higher resolution (1.25 and 1.05 Å, respectively), and the resolution of the C59S variant is the highest to date for any [2Fe-2S] protein. These structures confirm in each case the presence of a Ser Oγ-Fe2 bond that had been inferred previously from spectroscopic data (9, 13). More importantly, they reveal in considerable detail the conformational changes, in both the inorganic core and the polypeptide chain, that take place to accommodate the shortening of the Fe-Sγ bond upon replacement of sulfur by oxygen. The main structural perturbations observed in each case involve positional shifts of both Fe2 ligands, as well as adjustments to the nonplanarity of the Fe-S core. Interestingly, the structural rearrangements in the C55S and C59S variants differ in ways that are in keeping with the greater rigidity of the polypeptide chain around Cys-55.

The types of structural accommodations associated with changes observed for cluster ligands in Fd4 are also evident in more complex systems, such as nitrogenase. The P cluster of nitrogenase is a [8Fe-7S] metallocenter that exhibits structurally distinct oxidation states (39, 40). In the dithionite-reduced form assigned to the P^N oxidation state, the P cluster may be considered as two [4Fe-4S] clusters that share a common, hexacoordinate, sulfur. This assembly is coordinated to the nitrogenase MoFe-protein through six cysteine ligands, four of which coordinate a single iron, whereas the remaining two cysteines bridge two irons. In an oxidized form identified as the P^{OX} state, two of the irons move away from the central hexacoordinate sulfur, and these interactions are replaced with protein ligands, an amide nitrogen of one of the cluster cysteines and the side chain hydroxyl of Ser-β188. The structural rearrangements associated with the switch between these two forms of the P-cluster are primarily restricted to an increase in planarity of several Fe_2S_2 faces (Fig. 4) as the relevant Fe change positions; these correspond to an increase in the magnitude of the Fe–S-S-Fe torsion angles from ~145° in P^N (near that of [4Fe-4S] clusters) to ~175° in P^{OX} (near that of [2Fe-2S] clusters). Because these transitions are associated with little change in positions of the coordinating residues, the P^N to P^{OX} conversion more closely resembles the consequences for the [2Fe-2S] cluster geometry of serine ligation at residue Cys-55.

The high resolution structures of the C55S and C59S variants of *A. aeolicus* Fd4 may help illuminate a puzzling property of the counterpart C56S and C60S variants of the homologous protein from *C. pasteurianum*. In the one-electron reduced $[2Fe\text{-}2S]^+$ level, these mutated proteins, but not the WT, assume a delocalized mixed valence state resulting in a ground spin state $S = 9/2$, whereas in all other known cases, $[2Fe\text{-}2S]^+$ clusters display localized mixed valence states with an $S = 1/2$ ground spin state (14, 15). Although the structures reported here are those of the $[2Fe\text{-}2S]^{2+}$ redox level, they may nevertheless be used, with due caution, in the present discussion. Indeed, high resolution structures of both redox levels of a plant type Fd have shown that no major structural reorganization of the [2Fe-2S] cluster occurs upon reduction (5). The structural features favoring the appearance of the delocalized mixed valence pair may therefore be present, at least incipiently, in the $[2Fe\text{-}2S]^{2+}$ structures reported here. The distortion of the Fe_2S_2 inorganic core from planarity is unlikely to play a role because it is larger in C55S, and smaller in C59S, compared with WT (Table II). In contrast, the shortening of the Fe-Fe distance, albeit small (about 0.04 Å), is a unique feature of these serine-ligated [2Fe-2S] clusters. It should be noted that this shortening of the Fe-Fe distance is not a universal consequence of the substitution of Ser for Cys, however, as indicated by the slight increase in this distance in the Ser-49 variant of the *Anabaena* ferredoxin (34) and the absence of any significant change in the series of model compounds prepared by Coucouvanis and co-workers (41). It is feasible that this slight decrease in the Fe-Fe distance may favor the occurrence of the delocalized mixed valence state, especially because it is consistent with the prediction that transition from the localized to the delocalized valence state is determined by subtle structural modifications (15). Another potentially relevant feature occurs in both the WT and serine-ligated structures, namely, the unique distortion of the Cys-55 Sγ-Fe2-Sγ-Cys-59 moiety. Although this strain is likely to enhance the differences in coordination environment between the Fe1 and Fe2 sites in the WT protein, the Sγ/Oγ substitution may perhaps rebalance the electronic properties of Fe1 and Fe2 and thus favor the setup of double exchange and valence delocalization. These questions clearly beg for structural data on the reduced levels of both the WT and serine-ligated forms of *A. aeolicus* Fd4.

Sequence similarities indicate that several large redox enzymes, in particular hydrogenases and complex I of respiratory chains (1), contain subunits or domains that are predicted to assume structures similar to that of *A. aeolicus* Fd4. These subunits or domains presumably function as electron transfer agents and differ in at least two ways from *A. aeolicus* Fd4: (i) a single Fd-like module appears to be present, unlike the dimeric structure of Fd4, and (ii) the protruding loop in the vicinity of the [2Fe-2S] cluster is absent. The latter observation suggests that this loop in *A. aeolicus* Fd4 (and homologs in other bacteria, *e.g. C. pasteurianum* and *A. vinelandii*) may serve a possibly more sophisticated function than just electron transfer. In that respect, it should be emphasized that very rigid (near Cys-55) and more flexible (near Cys-59 or Cys-22) regions of the polypeptide chain, as well as a structurally constrained [2Fe-2S] metal site, are combined at the base of the protruding loop. This enhances the likelihood of tight interactions between the conformation of the polypeptide chain and the electronic structure (*e.g.* redox level) of the metal site. The role of these structural idiosyncrasies in the yet mysterious function of the thioredoxin-like [2Fe-2S] Fds will be the aim of future research.

Acknowledgments—Portions of this research were carried out at the Stanford Synchrotron Radiation Laboratory, a national user facility operated by Stanford University on behalf of the United States Department of Energy, Office of Basic Energy Sciences. The Stanford Synchrotron Radiation Laboratory Structural Molecular Biology Program is supported by the Department of Energy and the National Institutes of Health.

REFERENCES

1. Meyer, J. (2001) *FEBS Lett.* **509,** 1–5
2. Mortenson, L. E., Valentine, R. C., and Carnahan, J. E. (1962) *Biochem. Biophys. Res. Commun.* **7,** 448–452
3. Tagawa, K., and Arnon, D. I. (1962) *Nature* **195,** 537–543
4. Dauter, Z., Wilson, K. S., Sieker, L. C., Meyer, J., and Moulis, J. M. (1997) *Biochemistry* **36,** 16065–16073
5. Morales, R., Charon, M. H., Hudry-Clergeon, G., Pétillot, Y., Nørager, S., Medina, M., and Frey, M. (1999) *Biochemistry* **38,** 15764–15773
6. Golinelli, M. P., Chatelet, C., Duin, E. C., Johnson, M. K., and Meyer, J. (1998) *Biochemistry* **37,** 10429–10437
7. Chatelet, C., and Meyer, J. (1999) *J. Biol. Inorg. Chem.* **4,** 311–317
8. Chatelet, C., Gaillard, J., Pétillot, Y., Louwagie, M., and Meyer, J. (1999) *Biochem. Biophys. Res. Commun.* **261,** 885–889
9. Meyer, J., Fujinaga, J., Gaillard, J., and Lutz, M. (1994) *Biochemistry* **33,** 13642–13650
10. Golinelli, M. P., Akin, L. A., Crouse, B. R., Johnson, M. K., and Meyer, J. (1996) *Biochemistry* **35,** 8995–9002
11. Yeh, A. P., Chatelet, C., Soltis, S. M., Kuhn, P., Meyer, J., and Rees, D. C. (2000) *J. Mol. Biol.* **300,** 587–595
12. Chatelet, C., and Meyer, J. (2001) *Biochim. Biophys. Acta* **1549,** 32–36
13. Fujinaga, J., Gaillard, J., and Meyer, J. (1993) *Biochem. Biophys. Res. Commun.* **194,** 104–111
14. Crouse, B. R., Meyer, J., and Johnson, M. K. (1995) *J. Am. Chem. Soc.* **117,** 9612–9613
15. Achim, C., Golinelli, M. P., Bominaar, E. L., Meyer, J., and Münck, E. (1996) *J. Am. Chem. Soc.* **118,** 8168–8169
16. Bominaar, E. L., Achim, C., and Borshch, S. A. (1999) *J. Chem. Phys.* **110,** 11411–11422
17. Achim, C., Bominaar, E. L., Meyer, J., Peterson, J., and Münck, E. (1999) *J. Am. Chem. Soc.* **121,** 3704–3714
18. Otwinowski, Z., and Minor, W. (1997) *Methods Enzymol.* **276,** 307–326
19. Bailey, S. (1994) *Acta Crystallogr. Sect. D Biol. Crystallogr.* **50**, 760–763
20. Kissinger, C. R., Gehlhaar, D. K., and Fogel, D. B. (1999) *Acta Crystallogr. Sect. D Biol. Crystallogr.* **55**, 484–491
21. Brünger, A. T., Adams, P. D., Clore, G. M., DeLano, W. L., Gros, P., Grosse-Kunstleve, R. W., Jiang, J.-S., Kuszewski, J., Nilges, M., Pannu, N. S., Read, R. J., Rice, L. M., Simonson, T., and Warren, G. L. (1998) *Acta Crystallogr. Sect. D Biol. Crystallogr.* **54**, 905–921
22. Jones, T. A., Zou, J. Y., Cowan, S. W., and Kjeldgaard, M. (1991) *Acta Crystallogr. Sect. A* **47**, 110–119
23. Read, R. J. (1986) *Acta Crystallogr. Sect. A* **42**, 140–149
24. Sheldrick, G. M., and Schneider, T. R. (1997) *Methods Enzymol.* **277,** 319–343
25. Murshudov, G. N., Vagin, A. A., and Dodson, E. J. (1997) *Acta Crystallogr.* **53,** 240–255
26. Berg, J. M., and Holm, R. H. (1982) in *Iron Sulfur Proteins* (Spiro, T. G., ed) pp. 1–66, John Wiley & Sons, New York
27. Strop, P., Takahara, P. M., Chiu, H.-J., Hayley, C., Angove, C., Burgess, B.K., and Rees, D. C. (2001) *Biochemistry* **40,** 651–656
28. Colbert, C. L., Couture, M. M. J., Eltis, L. D., and Bolin, J. T. (2000) *Structure* **8,** 1267–1278
29. Iwata, S., Saynovits, M., Link, T. A., and Michel, H. (1996) *Structure* **4,** 567–579
30. Derewenda, Z. S., Lee, L., and Derewenda, U. (1995) *J. Mol. Biol.* **252,** 248–262
31. van Wart, H. E., and Scheraga, H. A. (1977) *Proc. Natl. Acad. Sci. U. S. A.* **74,** 13–17
32. Langen, R., Oh, K. J., Cascio, D., and Hubbell, W. L. (2000) *Biochemistry* **39,** 8396–8405
33. Bes, M. T., Parisini, E., Inda, L. A., Saraiva, L. M., Peleato, M. L., and Sheldrick, G. M. (1999) *Structure* **7,** 1201–1211
34. Hurley, J. K., Weber-Main, A. M., Hodges, A. E., Stankovich, M. T., Benning, M. M., Holden, H. M., Cheng, H., Xia, B., Markley, J. L., Genzor, C., Gomez-Moreno, C., Hafezi, R., and Tollin, G. (1997) *Biochemistry* **36,** 15109–15117
35. Xiao, Z. G., Lavery, M. J., Ayhan, M., Scrofani, S. D. B., Wilce, M. C. J., Guss, J. M., Tregloan, P. A., George, G. N., and Wedd, A. G. (1998) *J. Am. Chem. Soc.* **120,** 4135–4150
36. Meyer, J., and Moulis, J.-M. (2001) in *Handbook of Metalloproteins* (Messerschmidt, A., Huber, R., Poulos, T., and Wieghardt, K., eds) Vol. 1, pp. 505–517, John Wiley & Sons, Chichester, UK
37. Mansy, S. S., Xiong, Y., Hemann, C., Hille, R., Sundaralingam, M., and Cowan, J. A. (2002) *Biochemistry* **41,** 1195–1201
38. Rebelo, J. M., Dias, J. M., Huber, R., Moura, J. J. G., and Romao, M. J. (2001) *J. Biol. Inorg. Chem.* **6,** 791–800
39. Mayer, S. M., Lawson, D. M., Gormal, C. A., Roe, S. M., and Smith, B. E. (1999) *J. Mol. Biol.* **292,** 871–891
40. Peters, J. W., Stowell, M. H. B., Soltis, S. M., Finnegan, M. G., Johnson, M. K., and Rees, D. C. (1997) *Biochemistry* **36,** 1181–1187
41. Salifoglou, A., Simopoulos, A., Kostikas, A., Dunham, R. W., Kanatzidis, M. G., and Coucouvanis, D. (1988) *Inorg. Chem.* **27,** 3394–3406
42. Cruickshank, D. W. J. (1999) *Acta Crystallogr. Sect. D Biol. Crystallogr.* **55**, 583–601
43. Laskowski, R. A., MacArthur, M. W., Moss, D. S., and Thornton, J. M. (1993) *J. Appl. Crystallogr.* **26,** 283–291
44. Mayerle, J. J., Denmark, S. E., DePamphilis, B. V., Ibers, J. A., and Holm, R. H. (1975) *J. Am. Chem. Soc.* **97,** 1032–1045
45. Parisini, E., Capozzi, F., Lubini, P., Lamzin, V., Luchinat, C., and Sheldrick, G. (1999) *Acta Crystallogr. Sect. D Biol. Crystallogr.* **55**, 1773–1784